Early and not so early dark energy. What do cosmological observations tell us about them?

Adrià Gómez-Valent[1,*], Ziyang Zheng[1], Luca Amendola[1], Valeria Pettorino[2] and Christof Wetterich[1]

[1] *Institut für Theoretische Physik, Ruprecht-Karls-Universität Heidelberg, Philosophenweg 16, D-69120 Heidelberg, Germany*

[2] *AIM, CEA, CNRS, Université Paris-Saclay, Université Paris Diderot, Sorbonne Paris Cité F-91191 Gif-sur-Yvette, France*

Cosmological data still allow for the presence of a non-negligible amount of dark energy at very high redshifts, namely during the matter- and radiation-dominated epochs. This is the so-called early dark energy (EDE), which could help to mitigate the tensions that affect the standard model of cosmology since (i) it reduces the sound horizon at the baryon-drag epoch, hence giving room to higher values of H_0 than those found in the ΛCDM; and (ii) it could potentially decrease the number of large-scale structures in the Universe due its negative pressure and its inability to cluster efficiently for large enough values of its sound speed. Here we put constraints on the fraction of EDE using two methods: first, we use a perfect fluid parameterization that produces plateaux in $\Omega_{ede}(z)$ during the relativistic and non-relativistic matter-dominated eras. Second, we apply a tomographic approach to constrain the EDE density in redshift bins, which allows us to reconstruct the evolution of the EDE fraction before and after the decoupling of the Cosmic Microwave Background (CMB) photons. We have employed *Planck* data 2018, the Pantheon compilation of supernovae of Type Ia (SNIa), data on galaxy clustering, the prior on the absolute magnitude of SNIa by SH0ES, and weak lensing data from KiDS+VIKING-450 and DES-Y1. Using our minimal parameterization we find that EDE is not able to loosen the cosmological tensions, and show that the constraints on the EDE fraction weaken considerably when its sound speed takes lower values. Thanks to our binned analysis we are able to put tight constraints on the EDE fraction around the CMB decoupling time, $\lesssim 0.4\%$ at 2σ c.l. We confirm previous results that a significant EDE fraction in the radiation-dominated epoch loosens the H_0 tension, but tends to worsen the tension for σ_8. A subsequent presence of EDE in the matter-dominated era helps to alleviate this problem. When both the SH0ES prior and weak lensing data are considered in the fitting analysis in combination with data from CMB, SNIa and baryon acoustic oscillations, the EDE fractions are constrained to be $\lesssim 2.6\%$ in the radiation-dominated epoch and $\lesssim 1.5\%$ in the redshift range $z \in (100, 1000)$ at 2σ c.l. The two tensions remain with a statistical significance of $\sim 2-3\sigma$ c.l. This contribution to the proceedings of the CM3 parallel session of the MG16 Marcel Grossmann virtual Conference: "Status of the H_0 and σ_8 tensions: theoretical models and model-independent constraints" is based on the paper arXiv:2107.11065,[1] which appeared in the arXiv shortly after my talk of July 6th 2021.

Keywords: Cosmology: observations – Cosmology: theory – cosmological parameters – dark energy – dark matter.

*Speaker. E-mail: gomez-valent@thphys.uni-heidelberg.de

1. Introduction

The cosmological constant, Λ, is (together with other assumptions as the Cosmological Principle, the existence of cold dark matter (CDM) and an inflationary period prior to the radiation-dominated era) a key building block of the standard model of Cosmology. By adding this very simple term in Einstein's field equations it is possible to produce the late-time acceleration of the Universe[2,3] and help to explain a large variety of cosmological observations[4–6] without increasing excessively the mathematical complexity of the equations. However, the model is not free from extremely intricate theoretical conundrums, as the famous old cosmological constant[7–9] and coincidence problems, see e.g.[10] The former might be strongly intertwined with the latter, which should not be considered as a "why now" problem,[11] but as a matter of why the energy density associated to Λ, i.e. $\rho_\Lambda = \Lambda/8\pi G$, takes the value $\rho_\Lambda \sim \mathcal{O}(10^{-47})$ GeV^4 in natural units, hence being of the same order of magnitude of the non-relativistic matter energy density $\rho_m(z)$ when $z \lesssim 1$. This is pivotal for the model to exhibit an excellent phenomenological performance. We can soften the coincidence problem if we depart from the ΛCDM by allowing some sort of dynamical dark energy (DE) density instead of considering a rigid ρ_Λ.[12–14] This is a more appealing framework, since it is actually hard to believe in an immutable entity like the cosmological constant. Why should the component in charge of the current acceleration of the Cosmos be insensitive e.g. to the Universe's evolution and energy content? Such dynamics could lead to the presence of a non-negligible fraction of early dark energy (EDE) in the Universe during the radiation-dominated epoch (RDE) and/or the matter-dominated era (MDE). Of particular relevance concerning the coincidence problem are the quintessence models with scaling solutions, as the one with an exponential potential originally proposed by C. Wetterich in the late 80's,[14] in which the EDE fraction follows the dominant component in the Universe in both, the RDE and MDE,[15] making more natural the scenario with $\rho_{de} \sim \mathcal{O}(\rho_m)$ at low redshifts.

Apart from the aforementioned theoretical problems there are also some observational tensions affecting the ΛCDM, making the concordance model less concordant than it was thought to be ten years ago. At least, if these tensions are not induced by systematic errors in the data. The cosmic microwave background (CMB) temperature, polarization and lensing data from *Planck* 2018 leads to a value of the Hubble parameter $H_0 = (67.36 \pm 0.54)$ km/s/Mpc when analyzed under the assumption of the ΛCDM,[4] and a similar result is obtained from measurements of the baryon acoustic oscillations (BAO) and the deuterium abundance, again in the standard model.[16] These values are at odds with the one measured by the SH0ES team, $H_0 = (73.2 \pm 1.3)$ km/s/Mpc,[17] which is obtained with the cosmic distance ladder method and does not rely on the assumption of any cosmological model. There exists a $\sim 4.1\sigma$ tension between them, which has been persistently and consistently increasing in the last years,[18,19] see also the reviews.[20,21] On the other hand, galaxy clustering (through redshift-space distortions, RSD), direct peculiar velocity and

weak lensing (WL) measurements suggest that the Universe is less clumpy than preferred by the CMB data under the ΛCDM, see e.g.[22–25] The tension is usually formulated in terms of the root-mean-square (*rms*) of mass fluctuations at scales of $8h^{-1}$ Mpc, σ_8, and related composite quantities like $S_8 = \sigma_8(\Omega_m^{(0)}/0.3)^{0.5}$, with $\Omega_m^{(0)}$ the current matter energy fraction in the Universe. The first indication of its existence appeared already almost a decade ago[26] and it is still there.[27–29] The tension is in this case less significant from a statistical point of view than the aforesaid one of H_0, of about $2-3\sigma$ depending on the data source and the large-scale structure (LSS) estimator employed to quantify the tension. For instance, by combining the KiDS-1000 WL results with BOSS and 2dFLenS data the authors of[25] have shown that it is possible to reduce by a factor ~ 2 the uncertainty on S_8, and also to write the tension only in terms of σ_8, since BOSS puts tight constraints on $\Omega_m^{(0)}$ and the degeneracy in the $\sigma_8 - \Omega_m^{(0)}$ plane can be broken. They find $S_8 = 0.766^{+0.020}_{-0.014}$ and $\sigma_8 = 0.760^{+0.021}_{-0.023}$, which are in 3.1σ and 2.2σ tension with *Planck*, respectively.

Whether the H_0 and S_8/σ_8 tensions are to some degree physical or not is still unclear and under intense debate.[30–32] Hopefully this question will be resolved in the near future. In the meanwhile, theoreticians have worked very hard to find ways of loosening the tensions, taking for granted that they are real, see the reviews[21,33,34] and the complete lists of references therein. It is important to remark, though, that it is very difficult to find models in the literature capable of relieving both tensions at a time in a significant way. There are only some few exceptions that offer better perspectives, as e.g. the running vacuum model of type-II studied in[29] or the Brans-Dicke ΛCDM model explored in.[35,36] The latter, though, might encounter some problems when trying to match the cosmological and local values of the gravitational coupling through an appropriate screening mechanism,[37] and the effect of the *Planck* 2018 CMB polarization data might also hinder its overall fitting performance. Other models are only able to loosen one of the tensions, while worsening the other. This is the case e.g. of the class of new EDE models based on early phase transitions,[38–40] ultra-light axions[41,42] or alike.[43] In practice, all these models fight against the H_0 tension in a very similar way. There is a new component in the energy budget of the Universe that acts as a cosmological constant deep in the RDE and has an associated (constant) density which is of about $5-10\%$ the radiation energy density around the matter-radiation equality time, when the EDE fraction reaches its maximum. This excess of energy with respect to the standard model decreases the sound horizon at the baryon-drag epoch, and this forces the Hubble parameter to be larger in order to decrease the angular diameter distance to the last-scattering surface and keep in this way intact the location of the first peak of the temperature CMB anisotropies. The latter is very well constrained by *Planck*. After that moment, the energy density dilutes typically faster than radiation, leaving no imprint in the late-time universe, where a cosmological constant is still assumed to produce the current positive acceleration, as in the standard ΛCDM. Although it is possible to obtain posterior values of the Hubble parameter

much closer to the SH0ES measurement[17] in the context of these new EDE models, they require larger values of the current matter energy density in order to compensate the early Sachs-Wolfe effect introduced by EDE in the pre-recombination epoch, and this enhances the LSS formation processes in the late-time Universe, which in turn exacerbates the S_8/σ_8 tension.[44–46]

Here we first explore EDE models with scaling solutions in the MDE and RDE, or just in the MDE. As already discussed above, they can alleviate in some sense the coincidence problem. They could in principle have an impact on the cosmological tensions as well, depending on how strong are the constraints on the EDE fraction imposed by the the cosmological data. In these models, EDE might not be negligible after the recombination era, and this could lead to a softening of the S_8/σ_8 tension. Moreover, the shape of $\Omega_{ede}(z) = \rho_{ede}(z)/\rho_c(z)$, with $\rho_c(z) = 3H^2(z)/8\pi G$ the critical energy density in the Universe, is very different from the one encountered in the new EDE models mentioned in the previous paragraph, since in this case the EDE fraction is constant during the epochs at which the scaling behavior comes into play. Hence, it is clearly worth to study these EDE models and to determine to what extent they can alleviate the tensions, if they do at all. In view of the existing tensions, there is a clear interest of revisiting these models, whose seeds where already present more than thirty years ago.[14] In addition, we also perform a more model-independent analysis, applying a tomographic method to reconstruct the shape of $\Omega_{ede}(z)$ that is preferred by different combinations of cosmological data sets. We will see that this is very useful to extract more general information about how is EDE constrained in the various epochs of the cosmic expansion.

2. Early dark energy

EDE affects observables in several ways. The presence of EDE at decoupling can change the position and height of the peaks in the CMB[47–49] and can also impact it through the early integrated Sachs-Wolfe effect. Furthermore, EDE suppresses the growth of structure:[50–52] a smaller number of clusters can form with respect to the ΛCDM[53] because of the negative pressure of EDE and also because of its large sound speed, which does not allow it to cluster; the lensing potential is also weaker, with an impact on weak lensing and the CMB peaks at large multipoles. Thus, EDE can potentially have a direct impact on the cosmological tensions. In the following we first design a general parameterization able to mimic the background dominant component, and then proceed with a tomographic analysis in different redshift bins.

2.1. *Parametric EDE*

We build now a simple parameterization of the DE density that allows us to reproduce the behavior of uncoupled quintessence models with scaling solutions. For this reason, we want our parameterization to be able to generate two plateaux in $\Omega_{de}(z)$. The first plateau occurs in the RDE, and the second one in the MDE,

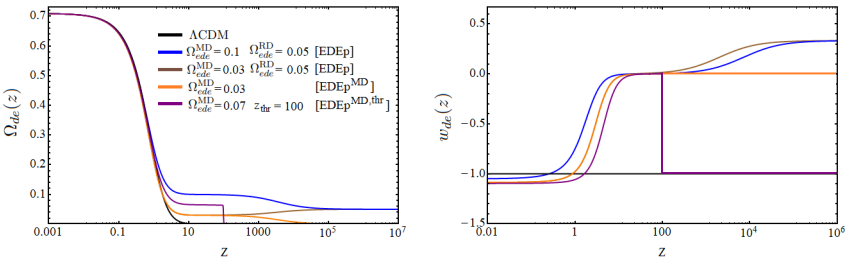

Fig. 1. Functions $\Omega_{de}(z)$ (left plot) and $w_{de}(z) = p_{de}(z)/\rho_{de}(z)$ (right plot) obtained using the parametrizations described in Sec. 2.1, for some illustrative values of the parameters.

and can have different heights in principle. This is what happens for instance in quintessence models with a single exponential potential $V(\phi) = V_0 e^{-\sqrt{8\pi G}\lambda\phi}$, where the fractions of EDE in the RDE and MDE depend only on one parameter, λ.[14,15] By introducing a second exponential potential it is possible to control the height of the two plateaux independently.[54]

With this aim in mind, we generalize the parameterizations proposed earlier in[48,49] and we consider here a DE density with the following form,

$$\rho_{de}(z) = \rho_1(1+z)^4 + \rho_2(1+z)^3 + \rho_3(1+z)^{3(1+w)}\,, \tag{1}$$

parameterized by the constant energy densities ρ_1, ρ_2 and ρ_3 and by a constant equation of state parameter (EoS) w. We call this parameterization EDEp, where the "p" reminds us of the 'plateaux' that characterise it. The last term of (1) is able to mimic the behavior of a late-time dynamical DE with the wCDM form,[55] whereas the first two terms produce the plateaux in the RDE and MDE. It is useful to write the constants ρ_1 and ρ_2 in terms of dimensionless parameters, as follows

$$\rho_1 = \chi_1 \Omega_{r,*}^{(0)} \rho_c^{(0)}\,; \qquad \rho_2 = \chi_2 \Omega_{m,*}^{(0)} \rho_c^{(0)}\,, \tag{2}$$

where $\Omega_{r,*}^{(0)}$ and $\Omega_{m,*}^{(0)}$ are the current density parameters of radiation and matter, respectively, computed considering three massless neutrinos, and $\rho_c^{(0)} = \rho_c(z=0)$. We consider standard General Relativity and a flat Friedmann-Lemaître-Robertson-Walker universe. $\chi_1, \chi_2, \rho_3 > 0$ in order the DE density to be positive during the expansion. Deep in the RDE and MDE the EDE fractions are constant,

$$\Omega_{ede}^{\rm RD} = \frac{\chi_1}{1+\chi_1}\,; \qquad \Omega_{ede}^{\rm MD} = \frac{\chi_2}{1+\chi_2}\,. \tag{3}$$

The present dark energy density, $\rho_{de}^{(0)}$, can be directly computed from the Hubble parameter, $H_0 = 100h$ km/s/Mpc, and the reduced CDM and baryon density parameters, $\omega_{cdm} = \Omega_{cdm}^{(0)} h^2$ and $\omega_b = \Omega_b^{(0)} h^2$. Thus, one of the three ρ_i's appearing in (1) can be expressed in terms of the other two, e.g. $\rho_3 = \rho_{de}^{(0)} - \rho_1 - \rho_2$, so in this EDE parametrization we deal with three additional parameters with respect to the ΛCDM. We have nine cosmological parameters in total, namely the spectral

index n_s and amplitude A_s of the primordial power spectrum, H_0, ω_b, ω_{cdm}, the optical depth to reionization, τ, together with w, χ_1 and χ_2 (or, equivalently, $\Omega_{ede}^{\rm RD}$ and $\Omega_{ede}^{\rm MD}$). We consider a massive neutrino of 0.06 eV and two massless neutrinos.

The DE fluid is covariantly conserved so its associated pressure reads,

$$\dot{\rho}_{de}+3H(\rho_{de}+p_{de})=0 \longrightarrow p_{de}(z)=\frac{\rho_1}{3}(1+z)^4+w\rho_3(1+z)^{3(1+w)}\,, \qquad (4)$$

where the dot refers to a derivative with respect to the cosmic time. The corresponding equation of state parameter can be obtained from the ratio of (4) and (1), i.e. $w_{de}(z)=p_{de}(z)/\rho_{de}(z)$. It is clear that $w_{de}=1/3$ and $w_{de}=0$ in the RDE and MDE, respectively, and $w_{de}\approx w$ at present for low values of χ_2. For the perturbations, in our main analyses we take the sound speed of the DE fluid to be equal to the speed of light in the DE rest frame,[56] i.e. $\hat{c}_s=1$, so in our model the DE does not cluster efficiently. We will study also what happens when $\hat{c}_s<1$.

If we set $\rho_1=0$ ($\Omega_{ede}^{\rm RD}=0$) in (1) EDE is completely negligible during the RDE,

$$\rho_{de}(z)=\rho_2(1+z)^3+\rho_3(1+z)^{3(1+w)}\,. \qquad (5)$$

We denote this particular case of EDEp as EDEp$^{\rm MD}$, to remind us that the plateau is in this case following the matter component. If we turn the first term on in (5) at a particular 'threshold' redshift $z_{\rm thr}$, in the MDE we obtain,

$$\rho_{de}(z)=\rho_2(1+z)^3\theta(z_{\rm thr}-z)+\rho_3(1+z)^{3(1+w)}\,, \qquad (6)$$

with θ the Heaviside step function. This is what we call EDEp$^{{\rm MD},thr}$. For $z_{\rm thr}\to\infty$ we recover the pure EDEp$^{\rm MD}$ parametrization (5). We show typical shapes of the functions $\Omega_{de}(z)$ and $w_{de}(z)$ obtained with EDEp, EDEp$^{\rm MD}$ and EDEp$^{{\rm MD},thr}$ in Fig. 1.

2.2. *Tomographic EDE*

We further consider the possibility of binning the amount of $\Omega_{de}(z)$ in 11 bins to perform a tomographic analysis using the data sets described in Sec. 3. Here, again, $\rho_{de}^{(0)}$ can be directly determined from H_0, ω_b and ω_{cdm}; the other constant densities ρ_i, with $i=A,...,J$ (see Table 1 in[1] for details), are left free in our Monte Carlo (MC) runs, together with w and the six usual ΛCDM parameters. We keep $\hat{c}_s=1$. Our main aim is to see how much EDE we can have in each bin, and therefore which shape of $\Omega_{de}(z)$ is preferred by the data, regardless of its complexity. The corresponding fitting results and reconstructed shapes of $\Omega_{de}(z)$ are shown and discussed in Sec. 4.2.

3. Methodology and data

We have implemented the various parametrizations of Sec. 2.1 and also the binned $\rho_{de}(z)$ described in Sec. 2.2 in our own modified version of the Einstein-Boltzmann code `CLASS`.[57] We have constrained the parameters of our models through a Bayesian

exploration of the parameter space, employing the MC sampler `MontePython`.[58] We have used flat priors for the cosmological parameters in common with the ΛCDM model, with widths that fully respect the *Planck* 2018 uncertainties.[4] Regarding the priors on the EDE fractions, previous studies in the literature showed that they are always lower than $\sim 10\%$,[48,49] so we have used $0 < \chi_i < 0.12$ in the MC analyses of the parametrizations of Sec. 2.1, and similar priors for each bin of the tomographic study of Sec. 2.2.

Now we list the various data sets used in this study:

- CMB: We consider the full *Planck* 2018 TTTEEE+lowE and TTTEEE+lowE+lensing likelihoods.[4] We denote these data sets as CMBpol and CMBpolens, respectively.
- Supernovae of Type Ia (SNIa): We use the observed SNIa apparent magnitude and redshifts of the Pantheon compilation.[5] The absolute magnitude of these SNIa, M, is left free in the fitting analysis, and we impose a prior on it. See the next item of the list for details.
- Prior on M: We use in some of our fitting analyses the SH0ES effective calibration prior on the absolute magnitude of the SNIa as provided in,[59] $M_{\rm SH0ES} = -19.2191 \pm 0.0405$. It is obtained from the calibration of nearby SNIa (at $z \lesssim 0.01$) with Cepheids.[60] It is better to use this prior rather than the one on H_0,[17,61] especially when it is combined with data from SNIa compilations that include the same SNIa in the Hubble flow considered by the SH0ES team (as in the Pantheon compilation[5]) because in this way we avoid double-counting issues. In some of our Tables we also provide the best-fit values of M. This allows us to quantity the 'M tension', i.e. the tension between the latter and $M_{\rm SH0ES}$. We show in Sec. 4.2 that the statistical level of the SH0ES-*Planck* tension can be in some cases quite different when formulated in terms of H_0 and M.
- BAO: We have employed the data reported in.[6,22,62–65]
- WL: In some of our fitting analyses we employ the KiDS +VIKING-450+DESY1 prior $S_8 = 0.762^{+0.025}_{-0.024}$.[66] The author of[67] has raised some concerns about the use of σ_8 and derived quantities as S_8. He suggests the use of σ_{12}, defined as the *rms* linear theory variance at the fixed scale of 12 Mpc, and $S_{12} = \sigma_{12}(\omega_m/0.14)^{0.4}$. We provide the values of these parameters in some of our Tables, together with the usual σ_8 and S_8.
- RSD: Data on anisotropic clustering of galaxies in redshift space, and from the direct measurement of peculiar velocities.[6,22,68–75] We call this data set RSD in short because most of these points are obtained from the analysis of redshift-space distortions.

The corresponding fitting results are presented and discussed in Sec. 4. In order to quantify the impact of the SH0ES prior on the fitting results and on the ability of the models to loosen the H_0/M tension we study and compare the constraints on our

Table 1. The mean fit values and 68.3% confidence limits for the ΛCDM, the wCDM, EDEp (1) and EDEp$^{\rm MD}$ (5), using the CMBpol+SNIa and CMBpolens+SNIa+M data sets (cf. Sec. 3). For $\Omega_{ede}^{\rm RD}$ and $\Omega_{ede}^{\rm MD}$ we also show the 2σ limits inside the parentheses. Constraints on τ are provided in.[1] See the comments in Sec. 4.1.

CMBpol+SNIa				
Parameter	ΛCDM	wCDM	EDEp	EDEp$^{\rm MD}$
ω_b	$0.02239^{+0.00014}_{-0.00015}$	$0.02237^{+0.00016}_{-0.00015}$	$0.02238^{+0.00017}_{-0.00016}$	$0.02234^{+0.00015}_{-0.00016}$
ω_{cdm}	$0.1199^{+0.0014}_{-0.0013}$	0.1204 ± 0.0014	$0.1218^{+0.0016}_{-0.0015}$	$0.1208^{+0.0014}_{-0.0015}$
n_s	0.9659 ± 0.0044	$0.9646^{+0.0044}_{-0.0045}$	$0.9642^{+0.0044}_{-0.0045}$	$0.9642^{+0.0043}_{-0.0046}$
H_0 [km/s/Mpc]	$67.60^{+0.59}_{-0.61}$	$68.55^{+1.12}_{-1.10}$	68.71 ± 1.16	$68.61^{+1.09}_{-1.16}$
σ_8	$0.811^{+0.007}_{-0.008}$	0.823 ± 0.014	$0.817^{+0.014}_{-0.015}$	$0.818^{+0.015}_{-0.014}$
r_d [Mpc]	$147.02^{+0.28}_{-0.32}$	146.92 ± 0.30	$146.18^{+0.66}_{-0.43}$	$146.75^{+0.36}_{-0.30}$
w	-1	$-1.039^{+0.035}_{-0.039}$	$-1.050^{+0.041}_{-0.040}$	$-1.053^{+0.038}_{-0.042}$
$\Omega_{ede}^{\rm RD}$ (%)	0	0	$< 0.91\,(< 2.08)$	0
$\Omega_{ede}^{\rm MD}$ (%)	0	0	$< 0.27\,(< 0.69)$	$< 0.29\,(< 0.69)$
CMBpolens+SNIa+M				
Parameter	ΛCDM	wCDM	EDEp	EDEp$^{\rm MD}$
ω_b	$0.02257^{+0.00015}_{-0.00014}$	$0.02241^{+0.00014}_{-0.00016}$	$0.02245^{+0.00015}_{-0.00019}$	0.02239 ± 0.00015
ω_{cdm}	0.1179 ± 0.0012	0.1200 ± 0.0015	0.1212 ± 0.0016	0.1206 ± 0.0012
n_s	0.9709 ± 0.0044	$0.9658^{+0.0044}_{-0.0047}$	$0.9659^{+0.0045}_{-0.0044}$	$0.9656^{+0.0041}_{-0.0042}$
H_0 [km/s/Mpc]	$68.56^{+0.56}_{-0.54}$	$70.55^{+0.86}_{-0.88}$	$70.63^{+0.86}_{-0.82}$	$70.20^{+0.52}_{-0.69}$
σ_8	$0.811^{+0.007}_{-0.008}$	0.838 ± 0.014	$0.830^{+0.014}_{-0.013}$	0.835 ± 0.010
r_d [Mpc]	$147.36^{+0.28}_{-0.29}$	$146.98^{+0.33}_{-0.30}$	$146.21^{+0.73}_{-0.44}$	146.79 ± 0.29
w	-1	$-1.098^{+0.035}_{-0.032}$	$-1.099^{+0.034}_{-0.032}$	$-1.099^{+0.030}_{-0.025}$
$\Omega_{ede}^{\rm RD}$ (%)	0	0	$< 1.14\,(2.44)$	0
$\Omega_{ede}^{\rm MD}$ (%)	0	0	$< 0.22\,(0.52)$	$< 0.22\,(0.54)$

EDE models obtained: (i) with a minimal data set composed by CMBpol+SNIa; and (ii) adding on top of the latter the SH0ES prior on M, i.e. using CMBpol+SNIa+M. The SNIa data help to break the strong degeneracies found in the w-H_0 plane when only CMB data are used in the analysis.[76]

The properties and limitations of the EDEp and EDEp$^{\rm MD}$ parametrizations are already grasped with the aforementioned minimal data sets (cf. Table 1). For EDEp$^{{\rm MD},thr}$ we study also the effect of the CMB lensing and BAO+RSD data when combined with CMBpol+SNIa. We provide the corresponding constraints in figures 2 and 3. For the analyses of the binned $\rho_{de}(z)$ described in Sec. 2.2 we report our results in Table 2, where we explicitly test the impact of BAO and the weak lensing data, by considering not only the minimal data sets described in the previous paragraph, but also adding the information on BAO and BAO+WL. In addition, we redo the fitting analyses considering also the CMB lensing in order to quantify

its impact. For further explanations on the data we refer the reader to our work[1] and the original data sources.

4. Results and discussion

We present and discuss now the results obtained from the fitting analyses of the EDE parametrizations and the tomographic EDE described in Secs. 2.1 and 2.2, respectively, using the methodology and data sets of the previous section.

4.1. *Results for the parametric analysis*

The mean fit values and corresponding uncertainties for the various cosmological parameters in the EDEp and EDEp$^{\rm MD}$ parametrizations obtained with the baseline CMBpol+SNIa dataset are reported in Table 1. The constraints on the fraction of early dark energy in the EDEp parametrization in the radiation- and matter-dominated epochs, $\Omega_{ede}^{\rm RD}$ and $\Omega_{ede}^{\rm MD}$, are very strong. They lie below $\sim 2\%$ and $\sim 0.7\%$, respectively, at the 2σ c.l. It is interesting to observe that the upper limit of $\Omega_{ede}^{\rm MD}$ in the EDEp$^{\rm MD}$ parametrization coincides with the one obtained in the more general EDEp. The constraints on $\Omega_{ede}^{\rm MD}$ and $\Omega_{ede}^{\rm RD}$ in EDEp are quite independent. Actually, we have checked that the correlation coefficient between these two parameters is pretty small, $\sim 5.6\%$. As already noticed in,[48] the low upper limits on $\Omega_{ede}^{\rm RD}$ and $\Omega_{ede}^{\rm MD}$ are due to the very tight constraint on the fraction of EDE around the CMB decoupling time. The latter acts as an anchor for $\Omega_{ede}^{\rm RD}$ and even more for $\Omega_{ede}^{\rm MD}$, since in the last scattering surface the matter energy density is already ~ 3 times larger than the radiation one.

Another result from Table 1 to remark is that EDEp cannot alleviate significantly the H_0 and σ_8 tensions. The shape of the early dark energy density seems to be too restricted in these parametrization. There is a slight increase of H_0 in EDEp and EDEp$^{\rm MD}$ with respect to the ΛCDM, but it is mainly due to the dynamics of the late-time DE, and this is why the major part of the effect is already found with the wCDM parametrization.[55]

When we include the SH0ES prior in our fitting analysis we increase, of course, the value of the Hubble parameter, see Table 1. The tension with the distance ladder determination is now only of $\sim 1.7\sigma$, but this is again mainly thanks to the lowering of w, which now lies more in the phantom region (3σ away below $w = -1$). The values of w and H_0 are almost identical to those found in the wCDM parametrization, and EDE does not have any important impact on the H_0 tension in the context of the EDEp parametrization. The loosening of the H_0 tension is accompanied by a slight worsening of the σ_8 one due to the positive correlation between H_0 and σ_8. Phantom dark energy leads to lower values of the DE density in the past and this produces, in turn, an increase of the structure formation processes in the Universe. It seems that the EDE density has a too restricted form in the parameterizations under study here. They allow for plateaux and generalize previous

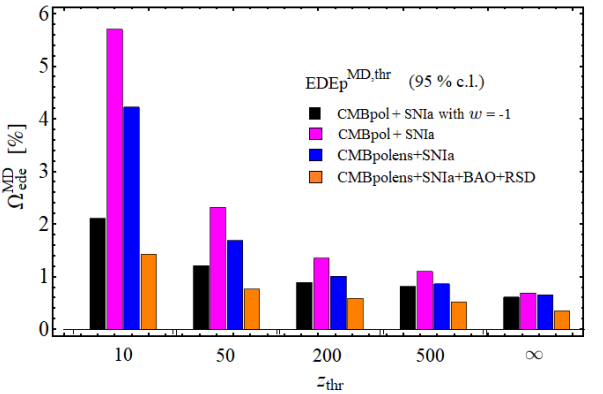

Fig. 2. Constraints on $\Omega_{ede}^{\rm MD}$ at 95% c.l. obtained from the fitting analyses of the EDEp$^{\rm MD,thr}$ parametrization (6), and under the data sets shown in the legend.

studies, but still seem to be quite constrained and unable to resolve the tensions. In the next section we then investigate the binned tomographic approach described in Sec. 2.2. Before moving on, however, we discuss briefly two options to weaken the constraints on the fraction of EDE.

Much weaker constraints on the fraction of EDE can be obtained by allowing for values of $\hat{c}_s^2 \ll 1$. The only difference between our EDE and cold dark matter during the MDE is found at the perturbations level. Both are pressureless fluids at the background level, but have different $\hat{c}_s$. The latter is equal to 1 for EDE and 0 for the dark matter. Hence, we expect the constraints on $\Omega_{ede}^{\rm MD}$ to loosen if we decrease the value of $\hat{c}_s$ of EDE, and even obtain a full degeneracy between the fraction of EDE and CDM during the MDE in the limit $\hat{c}_s \to 0$. This is actually what happens, as we explicitly show in Fig. 2 of.[1] We have to say, though, that the change in the sound speed does not help to alleviate the cosmological tensions, neither. For instance, under the CMBPol+SNIa data set the Hubble parameter remains close to ~ 67.5 km/s/Mpc, and the 1σ uncertainty is lower than ~ 0.8 km/s/Mpc regardless of the value of $\hat{c}_s$ under consideration when the late-time DE dynamics is switched off.

One can also get weaker constraints on EDE in the MDE by activating EDE at lower redshifts. In order to study this effect we explore the EDEp$^{{\rm MD},thr}$ parametrization (6). In Fig. 2 we provide the 2σ c.l. bounds on $\Omega_{ede}^{\rm MD}$ obtained with the baseline data set CMBpol+SNIa with and without late-time dark energy dynamics, and also adding the CMB lensing and the BAO+RSD data sets. When $z_{\rm thr} \to \infty$ we recover the constraints obtained in the EDEp$^{\rm MD}$ model, of course, but when we allow for lower values of the threshold redshift (below the CMB decoupling one) we get larger upper bounds on $\Omega_{ede}^{\rm MD}$, which depend on the concrete data set under consideration and also on $z_{\rm thr}$. We report the results obtained with $z_{\rm thr} = 10, 50, 200, 500, \infty$. The addition of the *Planck* 2018 CMB lensing to the CMBpol+SNIa baseline data set leads to stronger constraints on $\Omega_{ede}^{\rm MD}$. Its value decreases by a $\sim 25\%$ $\forall z_{\rm thr}$. When

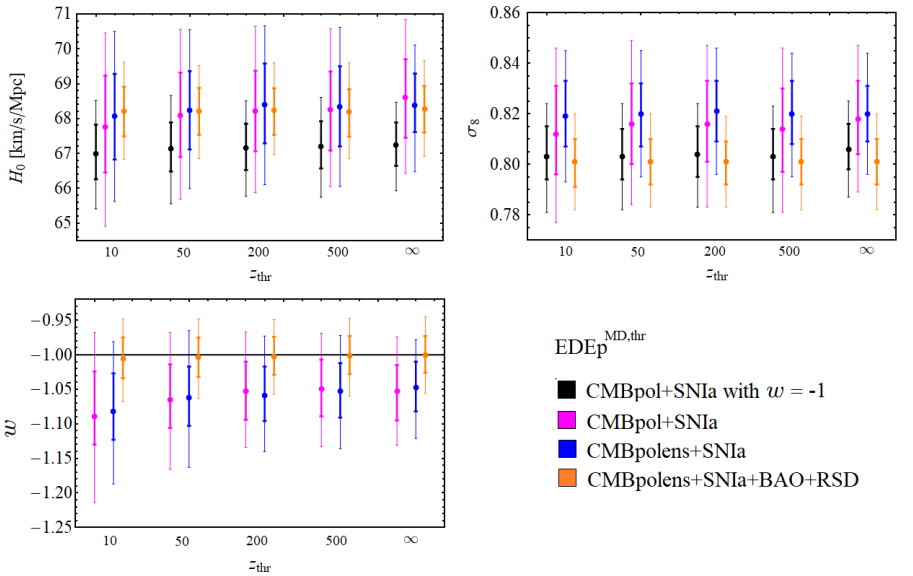

Fig. 3. Constraints for H_0, σ_8 and w at 1σ and 2σ c.l. obtained with the EDEp$^{\mathrm{MD},thr}$ parametrization (6) for different values of the threshold redshift z_{thr} and using the same combined data sets as in Fig. 2.

we also include the BAO+RSD data the decrease is even bigger, $\sim 75\%$. If we turn off the late-time dynamics of DE we also obtain tighter bounds on $\Omega_{ede}^{\mathrm{MD}}$, just because in this case we remove the degeneracy between this parameter and w. Our Fig. 2 can be compared with Figs. 6-7 of[48] and Fig. 11 of,[49] which were obviously obtained with older data sets. In[48] the authors employed CMB data from WMAP9 combined with small scale measurements from the South Pole Telescope (SPT), whereas in[49] the authors employed the *Planck* 2015 CMB likelihood and studied the impact of some other background and weak lensing data sets, as described in Sec. 4 in that reference. The results presented in this section constitute a significant update obtained with the *Planck* 2018 likelihood and also other more recent background and LSS data (cf. Sec. 3 for details).

In Fig. 3 we provide the corresponding constraints on H_0, σ_8 and w at 1σ and 2σ c.l. in the EDEp$^{\mathrm{MD,thr}}$ parameterization for the same scenarios explored in Fig. 2. They support some of the comments made in the previous paragraphs of this section, e.g. (i) the values of σ_8 and H_0 remain close to those found in the ΛCDM model. In other words, the tensions are not significantly alleviated in this class of scaling early dark energy models; (ii) phantom values of $w < -1$ allow us to decrease the H_0 tension very slightly; and (iii) larger values of w lead to lower values of σ_8 due to the presence of a larger fraction of dark energy at low redshifts. This is why we get $w \sim -1$ when we include the BAO+RSD data set.

The dedicated analysis presented in this section updated and generalized previous constraints on this class of early dark energy models, and motivated the study of

Table 2. The mean fit values and 68.3% confidence limits for the most important cosmological (main+derived) parameters, obtained under different data sets (with and without CMB lensing) for the binned $\rho_{de}(z)$ described in Sec. 2.2. See Fig. 4 for the constraints on $\Omega_{de}(z)$, and Sec. 4.2 for a thorough discussion on these results. Here we have employed the following notation: Base≡CMBpol+SNIa and BaseL≡CMBpolens+SNIa.

Parameter	Base	Base+M	Base+M+BAO	Base+M+BAO+WL
ω_b	$0.02257^{+0.00022}_{-0.00023}$	$0.02277^{+0.00023}_{-0.00025}$	$0.02282^{+0.00024}_{-0.00025}$	0.02259 ± 0.00021
ω_{cdm}	$0.1222^{+0.0020}_{-0.0021}$	0.1221 ± 0.0022	$0.1223^{+0.0020}_{-0.0021}$	$0.1200^{+0.0013}_{-0.0014}$
n_s	$0.9727^{+0.0072}_{-0.0073}$	$0.9752^{+0.0067}_{-0.0069}$	$0.9760^{+0.0070}_{-0.0071}$	$0.9740^{+0.0061}_{-0.0067}$
H_0 [km/s/Mpc]	$68.29^{+1.26}_{-1.36}$	$70.86^{+1.00}_{-1.10}$	$70.38^{+0.84}_{-0.89}$	$69.85^{+0.76}_{-0.77}$
M	-19.405 ± 0.032	$-19.342^{+0.023}_{-0.024}$	$-19.350^{+0.019}_{-0.020}$	$-19.365^{+0.018}_{-0.017}$
σ_8	$0.854^{+0.023}_{-0.025}$	$0.880^{+0.025}_{-0.029}$	$0.877^{+0.026}_{-0.029}$	$0.833^{+0.016}_{-0.017}$
S_8	$0.869^{+0.025}_{-0.029}$	0.863 ± 0.029	$0.866^{+0.026}_{-0.028}$	$0.819^{+0.014}_{-0.016}$
σ_{12}	$0.840^{+0.019}_{-0.022}$	0.843 ± 0.022	$0.843^{+0.020}_{-0.022}$	$0.806^{+0.012}_{-0.013}$
S_{12}	$0.851^{+0.022}_{-0.025}$	$0.854^{+0.024}_{-0.027}$	$0.855^{+0.023}_{-0.026}$	$0.810^{+0.014}_{-0.016}$
r_d [Mpc]	$145.66^{+0.90}_{-0.70}$	$145.22^{+0.95}_{-0.90}$	$145.06^{+0.97}_{-0.89}$	$146.51^{+0.64}_{-0.51}$
w	$-1.037^{+0.043}_{-0.041}$	-1.070 ± 0.038	$-1.048^{+0.037}_{-0.034}$	$-1.037^{+0.032}_{-0.031}$
Parameter	BaseL	BaseL+M	BaseL+M+BAO	BaseL+M+BAO+WL
ω_b	$0.02257^{+0.00021}_{-0.00023}$	$0.02274^{+0.00023}_{-0.00025}$	$0.02277^{+0.00022}_{-0.00024}$	$0.02266^{+0.00021}_{-0.00020}$
ω_{cdm}	0.1215 ± 0.0016	0.1211 ± 0.0017	0.1214 ± 0.0016	$0.1193^{+0.0013}_{-0.0014}$
n_s	$0.9721^{+0.0063}_{-0.0071}$	$0.9748^{+0.0067}_{-0.0071}$	$0.9746^{+0.0068}_{-0.0069}$	$0.9727^{+0.0061}_{-0.0068}$
H_0 [km/s/Mpc]	$68.25^{+1.27}_{-1.26}$	$70.84^{+1.04}_{-1.07}$	$70.21^{+0.80}_{-0.84}$	$70.00^{+0.76}_{-0.73}$
M	$-19.407^{+0.031}_{-0.030}$	$-19.343^{+0.024}_{-0.025}$	-19.355 ± 0.018	-19.362 ± 0.016
σ_8	$0.845^{+0.017}_{-0.020}$	$0.868^{+0.019}_{-0.021}$	$0.864^{+0.019}_{-0.021}$	$0.839^{+0.013}_{-0.015}$
S_8	$0.858^{+0.019}_{-0.021}$	$0.848^{+0.020}_{-0.022}$	$0.853^{+0.019}_{-0.020}$	$0.824^{+0.012}_{-0.013}$
σ_{12}	$0.831^{+0.014}_{-0.015}$	$0.831^{+0.015}_{-0.016}$	$0.833^{+0.015}_{-0.016}$	$0.810^{+0.010}_{-0.011}$
S_{12}	$0.841^{+0.016}_{-0.017}$	$0.840^{+0.017}_{-0.020}$	0.843 ± 0.018	$0.815^{+0.011}_{-0.013}$
r_d [Mpc]	$145.94^{+0.69}_{-0.57}$	$145.65^{+0.82}_{-0.71}$	$145.51^{+0.83}_{-0.71}$	$146.46^{+0.56}_{-0.44}$
w	$-1.035^{+0.040}_{-0.039}$	$-1.067^{+0.037}_{-0.036}$	$-1.050^{+0.034}_{-0.035}$	-1.045 ± 0.032

the next section, in which we will reconstruct the shape of $\Omega_{de}(z)$ without sticking to a restricted family of parametrizations.

4.2. *Results for tomographic dark energy*

Now we provide the results obtained in the tomographic model described in Sec. 2.2 in order to see whether more general shapes of $\Omega_{de}(z)$ can loosen the cosmological tensions. This is in fact suggested by previous analyses in the literature, see e.g.[38–43, 77]

Our results are presented in Table 2 and Fig. 4. They confirm that a significant (and non-constant) fraction of EDE in the RDE can alleviate the H_0 tension if it can be kept below $\sim 0.6\%$ at 2σ c.l. around the CMB decoupling time, i.e. at $z \sim 1000 - 2000$. For instance, from the analysis of the CMBpolens+SNIa and CMBpolens+SNIa+M+BAO data sets we obtain $H_0 = (68.25^{+1.27}_{-1.26})$ km/s/Mpc

and $H_0 = (70.21^{+0.80}_{-0.84})$ km/s/Mpc, respectively. They are 2.77σ and 1.95σ below the SH0ES measurement, and the central value is significantly lower when the SH0ES prior is not considered. The authors of[44] reported similar results in the context of the ultra-light axion model. Nevertheless, if we compare the values of M obtained from these data sets with $M_{\rm SH0ES}$ we still obtain a tension of 3.80σ and 3.07σ, respectively. This means that in terms of M, the tension is bigger than when it is formulated in terms of H_0, and the capability of EDE of alleviating the tension is much lower, at least in the EDE framework we are considering here.

We also see that the large fraction of $\Omega_{de}(z)$ required in the RDE to loosen the H_0 tension, which can be of about $\sim 4-5\%$ at 2σ c.l. according to some data sets that include the SH0ES prior on M but no LSS information, leads to higher values of ω_{cdm} and, to a lesser extent, also of n_s, which in turn exacerbates the σ_8/S_8 tension. The former is needed to reduce the early integrated Sachs-Wolfe effect introduced by the EDE. This is aligned with previous works that also consider EDE in the pre-recombination epoch, see e.g.[44–46,78,79] Table 2 shows that the tension decreases $\sim 1\sigma$ when it is analyzed through the LSS estimators σ_{12} and S_{12}.[67] Nevertheless, it does not disappear. Under the CMBpolens+SNIa+M data set the σ_8 tension is of 3.63σ, whereas for the σ_{12} parameter it is of 2.64σ, and a similar decrease is observed when other data combinations are employed in the fitting analysis.

When the SH0ES prior on M is taken into account in absence of LSS data, we get a $\sim 2\sigma$ evidence for the presence of a non-null EDE fraction during the RDE, similar to.[41] Nevertheless, the inclusion of the weak lensing data from KiDS+VIKING-450 and DES-Y1 (cf. Sec. 3) forces the EDE fraction in the RDE to be again compatible at 1σ with 0 in order to allow ω_{cdm} to take values closer to the ΛCDM ones and not to worsen the σ_8/S_8 tension. Notice that, as expected, the upper bound on the fraction of EDE in the MDE that we obtain in our binned analysis is larger than the one found with EDEp and its variants, even when the prior on S_8 is not included (see Table 1 and Fig. 4). Indeed, higher fractions of EDE in the MDE (see again Fig. 4) also allow to keep the amount of LSS more under control. With the CMBpolens+SNIa+M+BAO+WL we obtain $H_0 = (70.00^{+0.76}_{-0.73})$ km/s/Mpc and $M = -19.362 \pm 0.016$. They are in 2.13σ and 3.28σ tension with the SH0ES values, respectively. Again, the tension in M is larger than in H_0 by $\sim 1\sigma$. Regarding the LSS estimators, we obtain $S_8 = 0.824^{+0.012}_{-0.013}$ and $\sigma_{12} = 0.810^{+0.010}_{-0.011}$. The former is in 2.25σ tension with the KiDS+VIKING-450+DESY1 value, whereas the latter is compatible at 1σ with the value obtained in the ΛCDM. The tensions in H_0 and S_8 can be kept at $\sim 2\sigma$ c.l. under this concrete data set, as advocated in.[78]

The effect of the CMB lensing from *Planck* 2018 on the EDE fraction can be appreciated by direct comparison of the plots in the left and right columns of Fig. 4. When the CMB lensing is included, the upper bound on $\Omega_{de}(z)$ is reduced by $\sim 1\%$ for $z \gtrsim 5000$, by a $\sim 0.5\%$ for $3000 \lesssim z \lesssim 5000$ and by a smaller fraction at lower redshifts. Some differences are found, though, depending on the other data sets employed in the fitting analyses. The preferred matter densities decrease, although

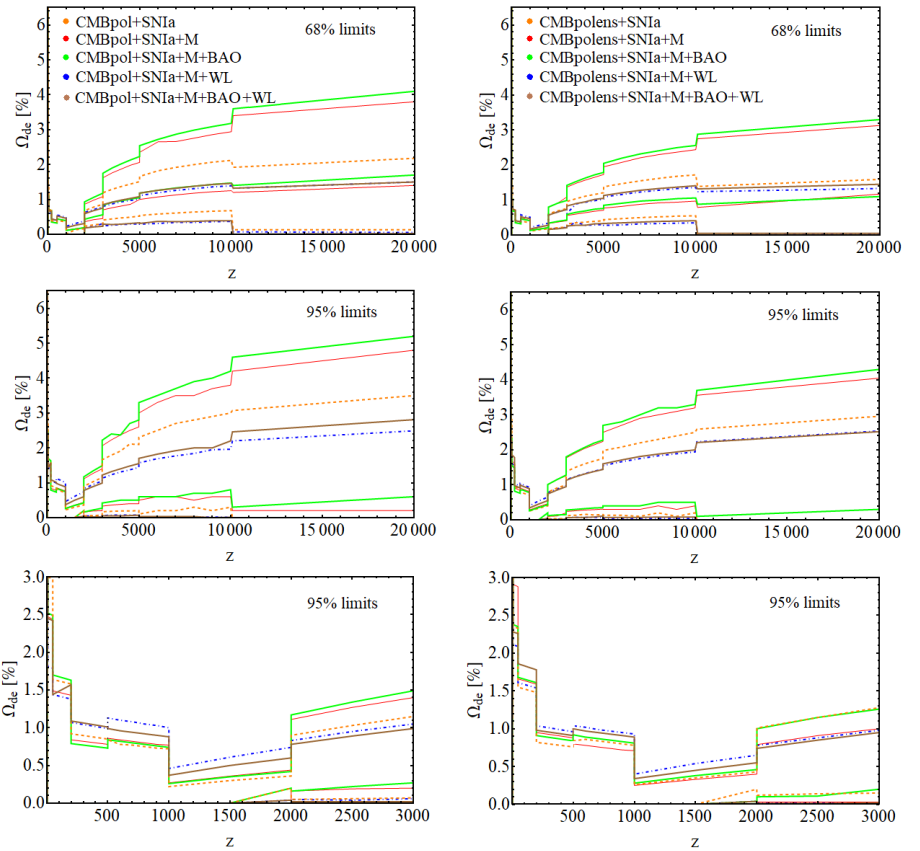

Fig. 4. *Left plots:* Reconstructed shapes of $\Omega_{de}(z)$ obtained from the fitting analyses without the Planck 2018 CMB lensing data (cf. Sec. 3). In the first and second rows we show the constraints in the region $z \in [0, 2 \cdot 10^4]$ at 1σ and 2σ c.l., respectively. In the last row we zoom in the redshift range $z \in [0, 3000]$ to better appreciate the details in the MDE. The tightest upper bound on $\Omega_{de}(z)$ is obtained around the CMB decoupling time, i.e. at $z \sim 1000 - 2000$, where the data force $\Omega_{de}(z) \lesssim 0.6\%$ at 2σ c.l.; *Right plots:* The same, but including the CMB lensing data. See the comments in Sec. 4.2.

they are still compatible at 1σ with the ones inferred without including the CMB lensing. This leads also to a slight decrease on the LSS estimators when the weak lensing prior is not considered. When the latter is included, the values of σ_{12} and S_{12} (and also σ_8 and S_8) remain stable under the addition of the CMB lensing likelihood.

We would like to remark the very low upper bounds that we obtain for the EDE fraction in the redshift range $z \in (1000, 2000)$, cf. Fig. 4. The exact value for these upper bounds depend on the specific data set, e.g. the constraints are a little bit weaker when the WL prior is used in the fitting analysis, but the EDE fraction when $\hat{c}_s = 1$ is, in any case, very strongly constrained in that epoch and lies always below $\sim 0.6\%$ regardless of the data set under consideration. Under the full data set, the

EDE fractions are constrained to be below 2.6% in the RDE and $\lesssim 1-1.5\%$ in the redshift range $z \in (100, 1000)$ at 2σ c.l. This limits strongly the possible impact of EDE on the value of the Hubble parameter or the present amount of structure.

5. Conclusions

In this work we have studied the phenomenological performance of a family of flexible parametrizations for the dark energy density that are able to mimic the scaling behavior that is encountered in a wide variety of quintessence models. DE has been treated as a perfect fluid with two plateaus in $\Omega_{de}(z)$, one in the matter-dominated epoch and another one in the radiation-dominated era. We have put very tight constraints on the fraction of EDE in the radiation- and matter-dominated epochs in the context of these models. The CMBpol+SNIa data set already forces these two quantities to lie below 2.44% and 0.52% at 2σ c.l., respectively. These strong constraints are necessary to respect the upper bound on the amount of EDE at the last scattering surface, as we have explicitly checked in our tomographic analysis. We have found that this class of scaling EDE models does not lead to a significant alleviation of the H_0 and σ_8 tensions. Larger EDE fractions are allowed by the data if: (i) the sound speed for DE is fixed at values $\hat{c}_s^2 \ll 1$, since in this limit dark energy behaves as dark matter during the matter-dominated epoch at the background and perturbations levels and, hence, there is a huge degeneracy between these two components. If we would assume a vanishing sound speed for dark energy there would be no way to distinguish it from dark matter. We find indeed no bounds on the dark energy fraction in this case. This changes drastically already for a rather small sound speed of EDE of the order 10^{-4}; and (ii) if EDE is switched on at later times, already in the matter-dominated era. Nevertheless, the cosmological tensions remain also in these cases.

EDE can only have a larger impact on the cosmological tensions if $\Omega_{de}(z)$ takes more flexible shapes that allow to respect the very strict constraints found around the CMB decoupling time ($\Omega_{de}(z_{dec}) \lesssim 0.4\%$ at 2σ c.l.), while still leading to a significant EDE fraction in other epochs of the cosmic expansion. The strong bound on EDE for redshift $200 < z < 1000$ ($\Omega_{de}(z) \lesssim 1\%$ at 2σ c.l.) is rather impressive since it is entirely based on the different clustering properties of dark energy and dark matter.

In general, when the SH0ES prior is not included in the fitting analysis there is no significant shift in the value of the Hubble parameter when compared to the ΛCDM, although the uncertainties clearly grow by a factor $2-3$. This allows to decrease the H_0 tension to the 2.66σ c.l. under the minimal CMBpol+SNIa data set. The addition of the CMB lensing has a very mild effect, increasing the tension up to the 2.73σ level.

When the BAO data and the SH0ES prior are also considered, the H_0 tension is reduced to the $\sim 2\sigma$ level by increasing the EDE fraction at the radiation-dominated epoch. A 2σ preference for a non-null EDE density in that epoch is obtained,

$\Omega_{de}(z) \lesssim 4\%$ at 95% c.l. Our reconstructed $\Omega_{de}(z)$ allows for non-peaked shapes, in contrast to what one finds e.g. in models based on ultra-light axions.[41,80] The model needs, though, values of the current dark matter density much larger than the ones typically encountered in the concordance model. This is to lower the early integrated Sachs-Wolfe effect down, which is enhanced by the presence of EDE in the pre-recombination epoch. This automatically leads to an increase of σ_8 and S_8 that worsens the LSS tension, which lies now at the $3 - 3.5\sigma$ c.l. In terms of σ_{12}, the tension is somewhat lower, but still remains at the $\sim 2.7\sigma$ level, as when the M prior is not used in the analysis. It is also to be noted that the H_0 tension still stays at the 3σ level when formulated in terms of the absolute magnitude of SNIa M.

Finally, when we use the most complete data set, taking also the weak lensing data into account, we find that the model can keep the H_0 and S_8 tensions at the $\sim 2\sigma$ c.l., thanks also to a slight increase of the EDE fraction in the matter-dominated epoch, although, again, the M tension remains at $\gtrsim 3\sigma$.

In view of our results, it seems unlikely that EDE alone can provide a satisfactory resolution of the cosmological tensions. Whether the latter have or not a physical origin, or whether their statistical significance is as high as claimed by some sectors of the cosmological community, is still a matter of discussion and is certainly not a closed subject. Here we conclude that, in any case, if the data sets employed in this study do not suffer from any important systematic errors, uncoupled EDE is not able to relieve completely the tensions. Under our full data set CMBpolens+SNIa+M+BAO+WL they remain at $2 - 3\sigma$ c.l.

Nothing prevents, though, the solution to the cosmological tensions to be multi-sided, rather than due to a single new physics component. EDE could still play a significant role in this story. Some interesting directions to explore in the future are: (i) a possible coupling of EDE to dark matter, (ii) the impact of more complicated behavior of the EDE sound speed, parameterizing its time dependence, or performing a tomographic analysis similar to the one we have carried out in this work for the EDE density; and (iii) the potential degeneracy between EDE and other cosmological parameters, as the neutrino masses, which could in principle help to soften the S_8 tension while keeping the needed amount of non-relativistic matter at the CMB decoupling time. The latter would be needed, together with a higher EDE fraction in the radiation-dominated epoch, in order to increase the value of the Hubble parameter. We leave these investigations for a future work.

Acknowledgments

The author is very grateful to Prof. Joan Solà Peracaula for his kind invitation to give this talk and co-chair the CM3 session with him. He was funded by the Deutsche Forschungsgemeinschaft (DFG) - Project number 415335479 - during the time at which the MG16 meeting was held and the research of this project carried out.

References

1. A. Gómez-Valent, Z. Zheng, L. Amendola, V. Pettorino and C. Wetterich, Early dark energy in the pre- and post-recombination epochs (7 2021).
2. S. Perlmutter *et al.*, Measurements of Ω and Λ from 42 high redshift supernovae, *Astrophys. J.* **517**, 565 (1999).
3. A. G. Riess *et al.*, Observational evidence from supernovae for an accelerating universe and a cosmological constant, *Astron. J.* **116**, 1009 (1998).
4. N. Aghanim *et al.*, Planck 2018 results. VI. Cosmological parameters, *Astron. Astrophys.* **641**, p. A6 (2020).
5. D. M. Scolnic *et al.*, The Complete Light-curve Sample of Spectroscopically Confirmed SNe Ia from Pan-STARRS1 and Cosmological Constraints from the Combined Pantheon Sample, *Astrophys. J.* **859**, p. 101 (2018).
6. R. Neveux *et al.*, The completed SDSS-IV extended Baryon Oscillation Spectroscopic Survey: BAO and RSD measurements from the anisotropic power spectrum of the quasar sample between redshift 0.8 and 2.2, *Mon. Not. Roy. Astron. Soc.* **499**, 210 (2020).
7. S. Weinberg, The Cosmological Constant Problem, *Rev. Mod. Phys.* **61**, 1 (1989), [,569(1988)].
8. J. Martin, Everything You Always Wanted To Know About The Cosmological Constant Problem (But Were Afraid To Ask), *Comptes Rendus Physique* **13**, 566 (2012).
9. J. Solà Peracaula, Cosmological constant and vacuum energy: Old and new ideas, *J. Phys. Conf. Ser.* **453**, p. 012015 (2013).
10. P. J. E. Peebles and B. Ratra, The Cosmological Constant and Dark Energy, *Rev. Mod. Phys.* **75**, 559 (2003).
11. H. E. S. Velten, R. F. vom Marttens and W. Zimdahl, Aspects of the cosmological "coincidence problem", *Eur. Phys. J. C* **74**, p. 3160 (2014).
12. P. J. E. Peebles and B. Ratra, Cosmology with a Time Variable Cosmological Constant, *Astrophys. J. Lett.* **325**, p. L17 (1988).
13. B. Ratra and P. J. E. Peebles, Cosmological Consequences of a Rolling Homogeneous Scalar Field, *Phys. Rev. D* **37**, p. 3406 (1988).
14. C. Wetterich, Cosmology and the Fate of Dilatation Symmetry, *Nucl. Phys. B* **302**, 668 (1988).
15. E. J. Copeland, A. R. Liddle and D. Wands, Exponential potentials and cosmological scaling solutions, *Phys. Rev. D* **57**, 4686 (1998).
16. G. E. Addison, D. J. Watts, C. L. Bennett, M. Halpern, G. Hinshaw and J. L. Weiland, Elucidating ΛCDM: Impact of Baryon Acoustic Oscillation Measurements on the Hubble Constant Discrepancy, *Astrophys. J.* **853**, p. 119 (2018).
17. A. G. Riess, S. Casertano, W. Yuan, J. B. Bowers, L. Macri, J. C. Zinn and D. Scolnic, Cosmic Distances Calibrated to 1% Precision with Gaia EDR3 Parallaxes and Hubble Space Telescope Photometry of 75 Milky Way Cepheids Confirm Tension with ΛCDM, *Astrophys. J. Lett.* **908**, p. L6 (2021).
18. A. G. Riess *et al.*, A 2.4% Determination of the Local Value of the Hubble Constant, *Astrophys. J.* **826**, p. 56 (2016).
19. A. G. Riess *et al.*, New Parallaxes of Galactic Cepheids from Spatially Scanning the Hubble Space Telescope: Implications for the Hubble Constant, *Astrophys. J.* **855**, p. 136 (2018).
20. L. Verde, T. Treu and A. G. Riess, Tensions between the Early and the Late Universe, *Nature Astron.* **3**, p. 891 (7 2019).
21. E. Di Valentino *et al.*, Snowmass2021 - Letter of interest cosmology intertwined II: The hubble constant tension, *Astropart. Phys.* **131**, p. 102605 (2021).

22. H. Gil-Marín, W. J. Percival, L. Verde, J. R. Brownstein, C.-H. Chuang, F.-S. Kitaura, S. A. Rodríguez-Torres and M. D. Olmstead, The clustering of galaxies in the SDSS-III Baryon Oscillation Spectroscopic Survey: RSD measurement from the power spectrum and bispectrum of the DR12 BOSS galaxies, *Mon. Not. Roy. Astron. Soc.* **465**, 1757 (2017).
23. S. Joudaki *et al.*, KiDS-450 + 2dFLenS: Cosmological parameter constraints from weak gravitational lensing tomography and overlapping redshift-space galaxy clustering, *Mon. Not. Roy. Astron. Soc.* **474**, 4894 (2018).
24. A. H. Wright, H. Hildebrandt, J. L. van den Busch, C. Heymans, B. Joachimi, A. Kannawadi and K. Kuijken, KiDS+VIKING-450: Improved cosmological parameter constraints from redshift calibration with self-organising maps, *Astron. Astrophys.* **640**, p. L14 (2020).
25. C. Heymans *et al.*, KiDS-1000 Cosmology: Multi-probe weak gravitational lensing and spectroscopic galaxy clustering constraints, *Astron. Astrophys.* **646**, p. A140 (2021).
26. E. Macaulay, I. K. Wehus and H. K. Eriksen, Lower Growth Rate from Recent Redshift Space Distortion Measurements than Expected from Planck, *Phys. Rev. Lett.* **111**, p. 161301 (2013).
27. S. Nesseris, G. Pantazis and L. Perivolaropoulos, Tension and constraints on modified gravity parametrizations of $G_{\rm eff}(z)$ from growth rate and Planck data, *Phys. Rev. D* **96**, p. 023542 (2017).
28. J. Solà Peracaula, J. de Cruz Pérez and A. Gómez-Valent, Possible signals of vacuum dynamics in the Universe, *Mon. Not. Roy. Astron. Soc.* **478**, 4357 (2018).
29. J. Solà Peracaula, A. Gómez-Valent, J. de Cruz Perez and C. Moreno-Pulido, Running vacuum against the H_0 and σ_8 tensions, *EPL* **134**, p. 19001 (2021).
30. G. Efstathiou, A Lockdown Perspective on the Hubble Tension (with comments from the SH0ES team) (7 2020).
31. E. Mortsell, A. Goobar, J. Johansson and S. Dhawan, The Hubble Tension Bites the Dust: Sensitivity of the Hubble Constant Determination to Cepheid Color Calibration (5 2021).
32. W. L. Freedman, Measurements of the Hubble Constant: Tensions in Perspective (6 2021).
33. E. Di Valentino *et al.*, Cosmology intertwined III: $f\sigma_8$ and S_8, *Astropart. Phys.* **131**, p. 102604 (2021).
34. E. Di Valentino, O. Mena, S. Pan, L. Visinelli, W. Yang, A. Melchiorri, D. F. Mota, A. G. Riess and J. Silk, In the realm of the Hubble tension—a review of solutions, *Class. Quant. Grav.* **38**, p. 153001 (2021).
35. J. Solà Peracaula, A. Gómez-Valent, J. de Cruz Pérez and C. Moreno-Pulido, Brans–Dicke Gravity with a Cosmological Constant Smoothes Out ΛCDM Tensions, *Astrophys. J. Lett.* **886**, p. L6 (2019).
36. J. Solà Peracaula, A. Gómez-Valent, J. de Cruz Pérez and C. Moreno-Pulido, Brans–Dicke cosmology with a Λ-term: A possible solution to ΛCDM tensions, *Class. Quant. Grav.* **37**, p. 245003 (2020).
37. A. Gómez-Valent and P. Hassan Puttasiddappa, Difficulties in reconciling non-negligible differences between the local and cosmological values of the gravitational coupling in extended Brans-Dicke theories (5 2021).
38. F. Niedermann and M. S. Sloth, New early dark energy, *Phys. Rev. D* **103**, p. L041303 (2021).
39. A. Gogoi, R. K. Sharma, P. Chanda and S. Das, Early Mass-varying Neutrino Dark Energy: Nugget Formation and Hubble Anomaly, *Astrophys. J.* **915**, p. 132 (2021).

40. F. Niedermann and M. S. Sloth, Resolving the Hubble tension with new early dark energy, *Phys. Rev. D* **102**, p. 063527 (2020).
41. V. Poulin, T. L. Smith, T. Karwal and M. Kamionkowski, Early Dark Energy Can Resolve The Hubble Tension, *Phys. Rev. Lett.* **122**, p. 221301 (2019).
42. T. L. Smith, V. Poulin and M. A. Amin, Oscillating scalar fields and the Hubble tension: a resolution with novel signatures, *Phys. Rev. D* **101**, p. 063523 (2020).
43. P. Agrawal, F.-Y. Cyr-Racine, D. Pinner and L. Randall, Rock 'n' Roll Solutions to the Hubble Tension (4 2019).
44. J. C. Hill, E. McDonough, M. W. Toomey and S. Alexander, Early dark energy does not restore cosmological concordance, *Phys. Rev. D* **102**, p. 043507 (2020).
45. M. M. Ivanov, E. McDonough, J. C. Hill, M. Simonović, M. W. Toomey, S. Alexander and M. Zaldarriaga, Constraining Early Dark Energy with Large-Scale Structure, *Phys. Rev. D* **102**, p. 103502 (2020).
46. G. D'Amico, L. Senatore, P. Zhang and H. Zheng, The Hubble Tension in Light of the Full-Shape Analysis of Large-Scale Structure Data, *JCAP* **05**, p. 072 (2021).
47. M. Doran, M. J. Lilley, J. Schwindt and C. Wetterich, Quintessence and the separation of CMB peaks, *Astrophys. J.* **559**, 501 (2001).
48. V. Pettorino, L. Amendola and C. Wetterich, How early is early dark energy?, *Phys. Rev. D* **87**, p. 083009 (2013).
49. P. A. R. Ade *et al.*, Planck 2015 results. XIV. Dark energy and modified gravity, *Astron. Astrophys.* **594**, p. A14 (2016).
50. P. G. Ferreira and M. Joyce, Structure formation with a selftuning scalar field, *Phys. Rev. Lett.* **79**, 4740 (1997).
51. M. Doran, J.-M. Schwindt and C. Wetterich, Structure formation and the time dependence of quintessence, *Phys. Rev. D* **64**, p. 123520 (2001).
52. R. R. Caldwell, M. Doran, C. M. Mueller, G. Schafer and C. Wetterich, Early quintessence in light of WMAP, *Astrophys. J. Lett.* **591**, L75 (2003).
53. M. Grossi and V. Springel, The impact of early dark energy on non-linear structure formation, *Mon. Not. Roy. Astron. Soc.* **394**, p. 1559–1574 (Apr 2009).
54. T. Barreiro, E. J. Copeland and N. J. Nunes, Quintessence arising from exponential potentials, *Phys. Rev. D* **61**, p. 127301 (2000).
55. M. S. Turner and M. J. White, CDM models with a smooth component, *Phys. Rev. D* **56**, p. R4439 (1997).
56. G. Ballesteros and J. Lesgourgues, Dark energy with non-adiabatic sound speed: initial conditions and detectability, *JCAP* **10**, p. 014 (2010).
57. D. Blas, J. Lesgourgues and T. Tram, The Cosmic Linear Anisotropy Solving System (CLASS) II: Approximation schemes, *JCAP* **07**, p. 034 (2011).
58. B. Audren, J. Lesgourgues, K. Benabed and S. Prunet, Conservative Constraints on Early Cosmology: an illustration of the Monte Python cosmological parameter inference code, *JCAP* **02**, p. 001 (2013).
59. D. Camarena and V. Marra, Local determination of the Hubble constant and the deceleration parameter, *Phys. Rev. Res.* **2**, p. 013028 (2020).
60. A. G. Riess, S. Casertano, W. Yuan, L. M. Macri and D. Scolnic, Large Magellanic Cloud Cepheid Standards Provide a 1% Foundation for the Determination of the Hubble Constant and Stronger Evidence for Physics beyond ΛCDM, *Astrophys. J.* **876**, p. 85 (2019).
61. M. J. Reid, D. W. Pesce and A. G. Riess, An Improved Distance to NGC 4258 and its Implications for the Hubble Constant, *Astrophys. J. Lett.* **886**, p. L27 (2019).

62. P. Carter, F. Beutler, W. J. Percival, C. Blake, J. Koda and A. J. Ross, Low Redshift Baryon Acoustic Oscillation Measurement from the Reconstructed 6-degree Field Galaxy Survey, *Mon. Not. Roy. Astron. Soc.* **481**, 2371 (2018).
63. E. A. Kazin *et al.*, The WiggleZ Dark Energy Survey: improved distance measurements to z = 1 with reconstruction of the baryonic acoustic feature, *Mon. Not. Roy. Astron. Soc.* **441**, 3524 (2014).
64. T. M. C. Abbott *et al.*, Dark Energy Survey Year 1 Results: Measurement of the Baryon Acoustic Oscillation scale in the distribution of galaxies to redshift 1, *Mon. Not. Roy. Astron. Soc.* **483**, 4866 (2019).
65. H. du Mas des Bourboux *et al.*, The Completed SDSS-IV Extended Baryon Oscillation Spectroscopic Survey: Baryon Acoustic Oscillations with Lyα Forests, *Astrophys. J.* **901**, p. 153 (2020).
66. S. Joudaki *et al.*, KiDS+VIKING-450 and DES-Y1 combined: Cosmology with cosmic shear, *Astron. Astrophys.* **638**, p. L1 (2020).
67. A. G. Sanchez, Arguments against using h^{-1}Mpc units in observational cosmology, *Phys. Rev. D* **102**, p. 123511 (2020).
68. K. Said, M. Colless, C. Magoulas, J. R. Lucey and M. J. Hudson, Joint analysis of 6dFGS and SDSS peculiar velocities for the growth rate of cosmic structure and tests of gravity, *Mon. Not. Roy. Astron. Soc.* **497**, 1275 (2020).
69. F. Simpson, C. Blake, J. A. Peacock, I. Baldry, J. Bland-Hawthorn, A. Heavens, C. Heymans, J. Loveday and P. Norberg, Galaxy and mass assembly: Redshift space distortions from the clipped galaxy field, *Phys. Rev. D* **93**, p. 023525 (2016).
70. C. Blake *et al.*, Galaxy And Mass Assembly (GAMA): improved cosmic growth measurements using multiple tracers of large-scale structure, *Mon. Not. Roy. Astron. Soc.* **436**, p. 3089 (2013).
71. C. Blake *et al.*, The WiggleZ Dark Energy Survey: the growth rate of cosmic structure since redshift z=0.9, *Mon. Not. Roy. Astron. Soc.* **415**, p. 2876 (2011).
72. F. G. Mohammad *et al.*, The VIMOS Public Extragalactic Redshift Survey (VIPERS): Unbiased clustering estimate with VIPERS slit assignment, *Astron. Astrophys.* **619**, p. A17 (2018).
73. L. Guzzo *et al.*, A test of the nature of cosmic acceleration using galaxy redshift distortions, *Nature* **451**, 541 (2008).
74. Y.-S. Song and W. J. Percival, Reconstructing the history of structure formation using Redshift Distortions, *JCAP* **10**, p. 004 (2009).
75. T. Okumura *et al.*, The Subaru FMOS galaxy redshift survey (FastSound). IV. New constraint on gravity theory from redshift space distortions at $z \sim 1.4$, *Publ. Astron. Soc. Jap.* **68**, p. 38 (2016).
76. G. Alestas, L. Kazantzidis and L. Perivolaropoulos, H_0 tension, phantom dark energy, and cosmological parameter degeneracies, *Phys. Rev. D* **101**, p. 123516 (2020).
77. A. Chudaykin, D. Gorbunov and N. Nedelko, Combined analysis of Planck and SPTPol data favors the early dark energy models, *JCAP* **08**, p. 013 (2020).
78. R. Murgia, G. F. Abellán and V. Poulin, Early dark energy resolution to the Hubble tension in light of weak lensing surveys and lensing anomalies, *Phys. Rev. D* **103**, p. 063502 (2021).
79. T. L. Smith, V. Poulin, J. L. Bernal, K. K. Boddy, M. Kamionkowski and R. Murgia, Early dark energy is not excluded by current large-scale structure data, *Phys. Rev. D* **103**, p. 123542 (2021).
80. V. Poulin, T. L. Smith, D. Grin, T. Karwal and M. Kamionkowski, Cosmological implications of ultralight axionlike fields, *Phys. Rev. D* **98**, p. 083525 (2018).